



## RESEARCH ARTICLE

[View Article Online](#)  
[View Journal](#) | [View Issue](#)

 Cite this: *Inorg. Chem. Front.*, 2023, 10, 2045

# LaAeAl<sub>3</sub>S<sub>7</sub> (Ae = Ca, Sr): Cairo pentagonal layered thioaluminates achieving a good balance between a strong second harmonic generation response and a wide bandgap†

 Jingjing Xu,<sup>b</sup> Kui Wu,<sup>b</sup> <sup>\*a</sup> Bingbing Zhang,<sup>b</sup> <sup>b</sup> Haohai Yu<sup>\*a</sup> and Huaijin Zhang<sup>\*a</sup>

Breaking through the incompatibility between a strong second harmonic generation (SHG) response and a wide bandgap in an infrared nonlinear optical (IR NLO) crystal is still a huge challenge. With this in mind, we have proposed a feasible design strategy involving rational combination of highly electropositive rare-earth (Re<sup>3+</sup>) and alkaline-earth metals (Ae<sup>2+</sup>) as cations and a strongly covalent AlS<sub>4</sub> anionic group as the "NLO-active unit" into the crystal structure, which affords the successful synthesis of two new quaternary IR NLO thioaluminates: LaAeAl<sub>3</sub>S<sub>7</sub> (Ae = Ca, Sr). Note that the unprecedented Cairo pentagonal (AlS<sub>4</sub>)<sub>n</sub> layers in LaAeAl<sub>3</sub>S<sub>7</sub> can be viewed as the first discovery among the structures of all reported thioaluminates and this layered structure benefits from the strong optical anisotropy that further achieves the imperative phase matchability in LaAeAl<sub>3</sub>S<sub>7</sub>. Both of them possess the widest optical bandgaps (Ca: 3.76 and Sr: 3.78 eV) in known rare-earth NLO chalcogenides. Remarkably, LaAeAl<sub>3</sub>S<sub>7</sub> were also proven to be the first cases concurrently exhibiting wide bandgaps (>3.5 eV) and strong SHG effects (>0.5 × AgGaS<sub>2</sub>) among known rare-earth NLO chalcogenides. Theoretical analysis verifies that their excellent NLO properties originate from the synergistic effect between AlS<sub>4</sub> and (La/Ae)S<sub>8</sub> anionic groups. This work will inspire exploration into new IR NLO candidates in rare-earth thioaluminate systems to achieve a superior property balance.

 Received 7th January 2023,  
 Accepted 21st February 2023

DOI: 10.1039/d3qi00048f

[rsc.li/frontiers-inorganic](https://rsc.li/frontiers-inorganic)

## Introduction

Nonlinear optical (NLO) crystals have shown extensive applications in tunable laser systems.<sup>1–15</sup> As for an excellent infrared (IR) NLO crystal, it should satisfy the following performance conditions: a wide IR transmission region, strong second harmonic generation (SHG) response, large optical bandgap, high laser damage threshold (LDT), and reliable chemical stability.<sup>16–18</sup> Unfortunately, there is still the undesirable incompatibility between the strong SHG response and wide bandgap in IR NLO crystals because of their inherent inverse relationship,<sup>19,20</sup> which is also reflected in several commercial crystals such as AgGaQ<sub>2</sub> (Q = S, Se)<sup>21</sup> and ZnGeP<sub>2</sub>.<sup>22</sup> They exhibit a good SHG response but relatively narrow energy

bandgaps and low LDTs, which further limit their application. Based on this, a good balance between a strong SHG response ( $d_{ij} > 0.5 \times \text{AgGaS}_2$ ) and wide bandgap ( $E_g > 3.5$  eV) has become an urgent challenge for the discovery of new excellent IR NLO crystals and many researchers have proposed several effective design strategies and research systems.<sup>23–29</sup> For example, mixed alkali/alkaline-earth metal sulfides possess wide bandgaps but relatively small SHG effects; introduction of halogen ions into the structures of typical chalcogenides means the mixed-anion chalcogenides can achieve a suitable property balance but the halides will corrode and destroy the silica tubes and further enhance the difficulty of the material synthesis. Considering the above status, we have focused on other research systems and thioaluminates exhibit native advantages to obtain a wide bandgap because their strongly covalent Al–S bond has a minor influence on optical absorption. However, up to now, thioaluminates have rarely been studied in NLO and only a few NLO thioaluminates have been reported for their NLO performances such as Al<sub>0.50</sub>Dy<sub>3</sub>(Si<sub>0.50</sub>Al<sub>0.50</sub>)S<sub>7</sub> (2.22 eV and 2 × KTiOPO<sub>4</sub> (KTP)), Al<sub>0.38</sub>Dy<sub>3</sub>(Si<sub>0.85</sub>Al<sub>0.15</sub>)S<sub>7</sub><sup>30,31</sup> (2.03 eV and 1 × KTP), BaAl<sub>4</sub>S<sub>7</sub><sup>32</sup> (3.95 eV and 0.5 × AgGaS<sub>2</sub>) and LiAlS<sub>2</sub><sup>33</sup> (5.13 eV and 0.2 × AgGaS<sub>2</sub>). Besides, the inherent relationship between the AlS<sub>4</sub> anionic group and the SHG

<sup>a</sup>State Key Laboratory of Crystal Materials and Institute of Crystal Materials, Shandong University, Jinan, China. E-mail: wukui@sdu.edu.cn, haohaiyu@sdu.edu.cn, huaijinzhang@sdu.edu.cn

<sup>b</sup>College of Chemistry and Environmental Science, Hebei University, Baoding, China  
 †Electronic supplementary information (ESI) available: Powder XRD, performance summary, crystal data, distortion degree. CCDC 2234185 for LaCaAl<sub>3</sub>S<sub>7</sub> and 2234186 for LaSrAl<sub>3</sub>S<sub>7</sub>, respectively. For ESI and crystallographic data in CIF or other electronic format see DOI: <https://doi.org/10.1039/d3qi00048f>

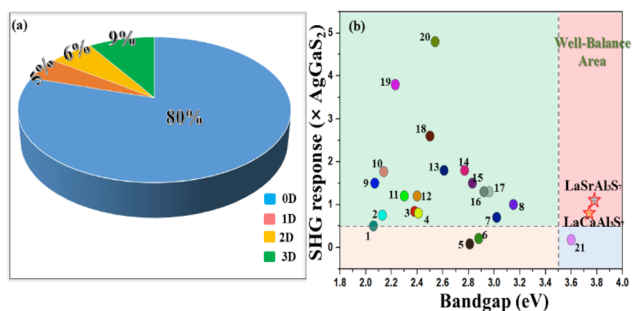


**Fig. 1** (a) Dimensional distribution of AlS<sub>4</sub> units in the known thioaluminates (Table S1†); (b) a summary of the SHG response and bandgap among the title LaAeAl<sub>3</sub>S<sub>7</sub> and reported rare-earth NLO chalcogenides, the well-balanced area is limited between E<sub>g</sub> > 3.5 eV and d<sub>ij</sub> > 0.5 × AgGaS<sub>2</sub>. Compounds 1–21 are listed in Table S2.†

origin has not been clearly determined so far. Recent study indicates that rare-earth centered polyhedral ReS<sub>n</sub> units make a great contribution to the origin of the NLO response, therefore, rare-earth based thioaluminates appear to have a high potentiality to break the incompatibility between the critical performances (E<sub>g</sub> and d<sub>ij</sub>) based on the synergistic effect between ReS<sub>n</sub> and AlS<sub>4</sub> units. With this in mind, we have proposed one design strategy involving rational combination of rare-earth (La<sup>3+</sup>) and alkaline-earth metals (Ae<sup>2+</sup>) as cations into the structures of thioaluminates to achieve the birth of two new rare-earth thioaluminates: LaAeAl<sub>3</sub>S<sub>7</sub> (Ae = Ca, Sr). Both of them exhibit the first examples of Cairo pentagon layers composed of AlS<sub>4</sub> tetrahedra in reported thioaluminates after a detailed survey of the Inorganic Crystal Structure Database (ICSD) (Fig. 1a) (Table S1†). Their performances were systematically measured and the results show that LaAeAl<sub>3</sub>S<sub>7</sub> were proven to be promising IR NLO materials because of the successful breakthrough in the incompatibility between the large E<sub>g</sub> (>3.5 eV) and strong d<sub>ij</sub> (>0.5 × AgGaS<sub>2</sub>). First-principles calculation analysis demonstrates that their SHG responses originate from the synergistic effect between AlS<sub>4</sub> and (La/Ae)S<sub>8</sub> units. Moreover, we have also summarized the critical properties (E<sub>g</sub> and d<sub>ij</sub>) in all known rare-earth chalcogenides (Fig. 1b) (Table S2†) and the survey results show that LaAeAl<sub>3</sub>S<sub>7</sub> could be regarded as the first cases achieving the breakthrough of the “3.5 eV wall” among all reported rare-earth NLO chalcogenides.<sup>31,34–48</sup>

## Experimental methods

### Synthesis

All raw materials, including La<sub>2</sub>S<sub>3</sub> powder (99.99%), Al slice (99.99%), CaS and SrS powder (99.99%), and S powder (99.99%), were purchased from Beijing Hawk Science & Technology Co., Ltd. As for air-unstable La<sub>2</sub>S<sub>3</sub>, SrS and CaS powder, an Ar-filled glovebox was selected to complete the whole preparation process.

Single crystals of LaAeAl<sub>3</sub>S<sub>7</sub> were firstly synthesized with a non-stoichiometric ratio based on the raw materials of La<sub>2</sub>S<sub>3</sub>,

CaS/SrS, Al, S = 0.37 : 1 : 3 : 3. However, under this ratio, the yield of LaAeAl<sub>3</sub>S<sub>7</sub> was very low and many AeAl<sub>2</sub>S<sub>4</sub> by-products were found. Thus, we gradually adjusted the proportion of raw materials after many attempts and the maximum yield (>90%) of LaAeAl<sub>3</sub>S<sub>7</sub> was obtained under the optimal nonstoichiometric ratio of La<sub>2</sub>S<sub>3</sub>, CaS/SrS, Al, S = 0.56 : 1 : 3 : 3. Raw materials were loaded into vacuum-sealed silica tubes and then put into a temperature-programmed furnace with the following temperature controlling curves: heated up to 1473 K within 30 h and held for 90 h, then cooled to room temperature within 150 h. The transparent and colorless LaAeAl<sub>3</sub>S<sub>7</sub> single crystals were obtained.

### Single crystal X-ray diffraction

Selected high-quality crystals were used for data collection on a Bruker D8 VENTURE diffractometer using Mo K $\alpha$  radiation ( $\lambda$  = 0.71073 Å) at room temperature. A multi-scan method was used for absorption correction. The crystal structures were solved by a direct method and refined using the SHELXTL program package. After the first refinement, the formula was firstly refined to be the unbalanced “La<sub>2</sub>Al<sub>3</sub>S<sub>7</sub>”. The occupancy of La and Ca atoms in one site appeared to be 0.49 : 0.51 after the first random refinement. In order to obtain the balanced formula, we defined the actual occupancy of La and Ca atoms to be 0.5 : 0.5 and the final balanced formula is LaCaAl<sub>3</sub>S<sub>7</sub>. Similarly, this refinement process was extended to those of LaSrAl<sub>3</sub>S<sub>7</sub> in this work. Rational anisotropic thermal parameters for all atoms were obtained by the anisotropic refinement and extinction correction. Detail refinement parameters and crystal data are shown in Table S3.†

### Powder X-ray diffraction

Powder X-ray diffraction (PXRD) patterns were collected on a Bruker D2 X-ray diffractometer with Cu K $\alpha$  radiation ( $\lambda$  = 1.5418 Å) at room temperature. The 2 $\theta$  range was 10–70° with a step size of 0.02° and a fixed counting time of 1 s per step. Note that the calculated XRD patterns were derived from the respective single-crystal data. We have also carefully investigated the experimental XRD patterns of the title compounds and compared the extra peaks with those of other known related compounds.

### UV-Vis-Near-IR (NIR) diffuse-reflectance spectra

Diffuse-reflectance spectra were measured by a Shimadzu SolidSpec-3700DUV spectrophotometer in the wavelength range of 200–1100 nm at room temperature.

### Raman spectra

Hand-picked crystals were firstly put on a glass slide and then a LABRAM HR Evolution spectrometer equipped with a CCD detector by a 532 nm laser was used to record the Raman spectra.

### Second-harmonic generation measurement

Through the Kurtz and Perry method, powder SHG responses were investigated by a Q-switch laser (2.09  $\mu$ m, 3 Hz, 50 ns)

with different particle sizes, including 38–55, 55–88, 88–105, 105–150, 150–200, and 200–250  $\mu\text{m}$ . The as-synthesized AgGaS<sub>2</sub> microcrystals were selected with the same sizes as references.

### Theory calculations

In order to further investigate the relationship of structure–property, the electronic structures of the title compounds were studied by density functional theory (DFT) based on *ab initio* calculations. The exchange–correlation potential was calculated using the Perdew–Burke–Ernzerhof (PBE) functional within the generalized gradient approximation (GGA) with the scheme. The following orbital electrons were treated as valence electrons: La: 5s<sup>2</sup> 5p<sup>6</sup> 5d<sup>1</sup> 6s<sup>2</sup>; Ca: 3p<sup>6</sup> 4s<sup>2</sup>; Sr: 4p<sup>6</sup> 5s<sup>2</sup>; Al: 3s<sup>2</sup> 3p<sup>1</sup>; S: 3s<sup>2</sup> 3p<sup>4</sup>. To achieve energy convergence, the plane-wave basis set energy cutoff was 660 eV within normal-conserving pseudo-potential (NCP). As key parameters for NLO crystals, the SHG coefficient and birefringence were also calculated. Owing to the discontinuity of exchange correlation energy, the experimental value is usually larger than that of the calculated band gap. Thus, scissors operators are used to make the conduction bands agree with the experimental values and the real-space atom-cutting method was used to analyse the contribution of anionic groups.

## Results and discussion

In this work, single crystals of title LaAeAl<sub>3</sub>S<sub>7</sub> thioaluminates were synthesized with an optimized nonstoichiometric ratio after many attempts. Submillimeter-level single-crystals were handpicked to be used for the data collection on single-crystal XRD (Table S3<sup>†</sup>). The phase-purity was verified by a powder XRD technique (Fig. S1<sup>†</sup>). The experimental PXRD patterns are basically consistent with those of the theoretical ones and a few extra tiny peaks are attributed to the AeAl<sub>2</sub>S<sub>4</sub> by-products.

LaAeAl<sub>3</sub>S<sub>7</sub> (Ae = Ca, Sr) crystallize in the  $P\bar{4}2_1m$  space group of the tetragonal system. In view of their similar structures, LaCaAl<sub>3</sub>S<sub>7</sub> was selected as the representative to depict their structural features. La and Ca atoms are located at the one site with the occupied ratio (0.5 : 0.5). One AlS<sub>4</sub> unit is linked to four AlS<sub>4</sub> units to form a [Al<sub>5</sub>S<sub>16</sub>]<sup>17-</sup> windmill cluster and these clusters further link together to compose the 2D Cairo pentagonal layers located at the *ab* plane. (La/Ca)S<sub>8</sub> polyhedra were located within the interlayers to bridge adjacent layers together to compose the overall 3D network. In this work, various link modes of AlS<sub>4</sub> units in structures of thioaluminates were also summarized and most of them (about 80%) possess the 0D link modes after the survey in the ICSD (Fig. 1a) (Table S1<sup>†</sup>). In addition, only three of the thioaluminates (Rb<sub>4</sub>Al<sub>2</sub>S<sub>5</sub>,<sup>49</sup> Bi<sub>2</sub>Al<sub>4</sub>S<sub>8</sub><sup>50</sup> and *Cccm*-SrAl<sub>2</sub>S<sub>4</sub><sup>51</sup>) exhibit 1D (AlS<sub>4</sub>)<sub>n</sub> chains but the link modes of the AlS<sub>4</sub> units in the 1D chains are different, for example, AlS<sub>4</sub> units connect with each other by edge-sharing to form similar 1D chains in Bi<sub>2</sub>Al<sub>4</sub>S<sub>8</sub> (Fig. S2a and b<sup>†</sup>) and *Cccm*-SrAl<sub>2</sub>S<sub>4</sub> (Fig. S2e and f<sup>†</sup>), which is different to the way AlS<sub>4</sub> units link together by edge and corner-sharing to

form a 1D chain structure in Rb<sub>4</sub>Al<sub>2</sub>S<sub>5</sub> (Fig. S2c and d<sup>†</sup>). Note that the ratio of the 3D network is only 9% and seven of them possess 3D networks formed by AlS<sub>4</sub> units. For instance, AlS<sub>4</sub> units link together by corner-sharing to form a 3D network and Ba atoms are located within the 3D tunnels to form the whole structure of BaAl<sub>4</sub>S<sub>7</sub> (Fig. S3c<sup>†</sup>). In particular, Al atoms have two different coordination modes: AlS<sub>4</sub> and AlS<sub>6</sub> units in the structure of Ln<sub>6</sub>Al<sub>3.3</sub>S<sub>14</sub><sup>52</sup> and AlS<sub>6</sub> units link together by sharing faces to form a 1D chain structure and AlS<sub>4</sub> units are existed in isolation (Fig. S3a and b<sup>†</sup>). Note that 2D (AlS<sub>4</sub>)<sub>n</sub> layers were also rarely discovered and only a few ternary thioaluminates exhibit 2D layered structures, such as FeAl<sub>2</sub>S<sub>4</sub>,<sup>53</sup> TlAlS<sub>2</sub><sup>54</sup> and AeAl<sub>2</sub>S<sub>4</sub><sup>55</sup> (Ae = Ca, Sr). Although they have layered structures, the link modes of their AlS<sub>4</sub> units are different to those in the title LaAeAl<sub>3</sub>S<sub>7</sub> (Fig. 2b and e). Therefore, the Cairo pentagonal layers in the title LaAeAl<sub>3</sub>S<sub>7</sub> can be viewed as the first discovery in the known thioaluminates. For instance, 6-membered rings (MRs) exist in the structure of CaAl<sub>2</sub>S<sub>4</sub> and its interlayer spacing (1.654 Å) is smaller

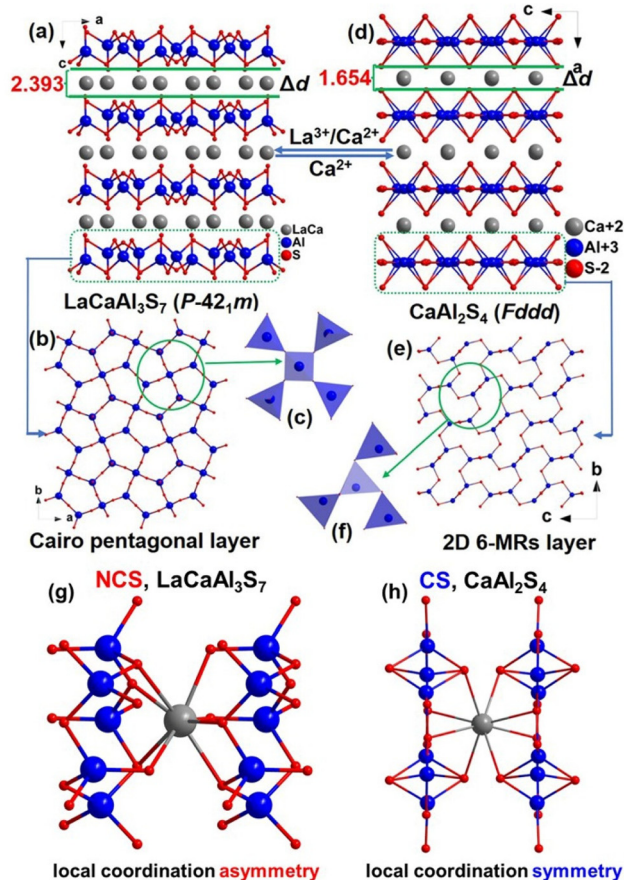


**Fig. 2** (a) The crystal structure of LaCaAl<sub>3</sub>S<sub>7</sub> along the *b*-axis; (b) the 2D layer is composed of AlS<sub>4</sub> units in LaCaAl<sub>3</sub>S<sub>7</sub>; (c) the windmill configuration [Al<sub>5</sub>S<sub>16</sub>]<sup>17-</sup> cluster; (d) the crystal structure of CaAl<sub>2</sub>S<sub>4</sub> along the *b*-axis; (e) the 2D layer is composed of AlS<sub>4</sub> units in CaAl<sub>2</sub>S<sub>4</sub>; (f) the connection mode of AlS<sub>4</sub> unit in CaAl<sub>2</sub>S<sub>4</sub>; (g) the local coordination asymmetry between (La/Ca)S<sub>8</sub> and AlS<sub>4</sub> units in LaCaAl<sub>3</sub>S<sub>7</sub>; and (h) the local coordination symmetry between CaS<sub>8</sub> and AlS<sub>4</sub> in CaAl<sub>2</sub>S<sub>4</sub>.

than that of  $\text{LaCaAl}_3\text{S}_7$  (2.393 Å) (Fig. 2a and d). Besides,  $\text{AlS}_4$  is connected with three  $\text{AlS}_4$  units in  $\text{CaAl}_2\text{S}_4$  which is different to the  $[\text{Al}_5\text{S}_{16}]^{17-}$  windmill cluster in the  $\text{LaCaAl}_3\text{S}_7$  (Fig. 2c and f). Moreover, one  $(\text{La}/\text{Ca})\text{S}_8$  is linked to ten  $\text{AlS}_4$  units but the inherent link modes are different and not symmetrical, showing local asymmetry in the  $\text{LaCaAl}_3\text{S}_7$ , which is also different to that (local coordination symmetry) in the  $\text{CaAl}_2\text{S}_4$  (Fig. 2g and h). We have also calculated the distortion degrees ( $\Delta d$ ) of  $(\text{La}/\text{Ae})\text{S}_8$  in the  $\text{LaAeAl}_3\text{S}_7$  and  $\text{AeS}_8$  dodecahedra in  $\text{AeAl}_2\text{S}_4$  (Table S4†) and the results show that  $(\text{La}/\text{Ae})\text{S}_8$  have a larger  $\Delta d$  (Sr: 2.763‰; Ca: 2.686‰) in  $\text{LaAeAl}_3\text{S}_7$  than those of  $\text{SrS}_8$  (0.030–0.092‰) and  $\text{CaS}_8$  (0.0007–0.140‰) in  $\text{AeAl}_2\text{S}_4$ . Such a large  $\Delta d$  is beneficial to achieve the local coordination asymmetry and promotes a potential structural change from centrosymmetric (CS)  $\text{AeAl}_2\text{S}_4$  to NCS  $\text{LaAeAl}_3\text{S}_7$ .

Diffuse-reflectance spectra of  $\text{LaAeAl}_3\text{S}_7$  were measured and their optical bandgaps are 3.76 eV for  $\text{LaCaAl}_3\text{S}_7$  and 3.78 eV for  $\text{LaSrAl}_3\text{S}_7$ , respectively (Fig. 3a and b), which are much larger than that of commercial  $\text{AgGaS}_2$  (2.64 eV) and comparable to other famous NLO crystals such as  $\text{BaAl}_4\text{S}_7$ <sup>32</sup> (3.95 eV),  $\text{LiZnPS}_4$ <sup>56</sup> (3.44 eV),  $\text{K}_3\text{Ga}_3\text{PS}_8\text{Cl}$ <sup>57</sup> (3.60 eV),  $\text{BaGa}_2\text{SiS}_6$ <sup>58</sup> (3.75 eV) and  $\text{Li}_2\text{ZnSiS}_4$ <sup>59</sup> (3.90 eV). Note that  $\text{LaAeAl}_3\text{S}_7$  exhibit the widest optical bandgaps and they can be also viewed as the first cases to achieve the breakthrough of “3.5 eV wall” in all the reported rare-earth NLO chalcogenides. Analysis into the calculated electronic structures and density of states (DOS) shows that the title  $\text{LaAeAl}_3\text{S}_7$  are indirect-bandgap compounds and their theoretical bandgaps are 2.505 eV for  $\text{LaCaAl}_3\text{S}_7$  and 2.527 eV for  $\text{LaSrAl}_3\text{S}_7$ , respectively (Fig. 3c and d). As can

be seen from their DOS diagrams, the top of the valence band (VB) and the bottom of the conduction band (CB) region are mainly occupied by the S-p and La-d with a minor contribution of Al-p orbitals and Ae-s,p orbitals producing a negligible effect on the optical bandgaps. Therefore, optical absorptions in  $\text{LaAeAl}_3\text{S}_7$  are determined by the inherent electronic transition in La-S units (Fig. 3e and f). Note that the wide bandgap has a huge influence on improving the inherent laser damage threshold (LDT), thus, their LDTs were measured under the 1.06 μm laser with the commercial  $\text{AgGaS}_2$  as reference. Both of them have a high laser damage resistance of about 9.0 times that of  $\text{AgGaS}_2$ , which are comparable to those of IR NLO sulfides such as  $\text{KYGes}_4$ <sup>39</sup> ( $10 \times \text{AgGaS}_2$ ),  $\text{LiGaGe}_2\text{S}_6$ <sup>60</sup> ( $6 \times \text{AgGaS}_2$ ),  $\text{Li}_2\text{ZnSiS}_4$ <sup>59</sup> ( $10 \times \text{AgGaS}_2$ ) and  $\text{Li}_{0.6}\text{Ag}_{0.4}\text{GaS}_2$ <sup>61</sup> ( $8.6 \times \text{AgGaS}_2$ ). The measured Raman spectra exhibit no obvious absorption peaks in the wavenumber range from 500 to 4000  $\text{cm}^{-1}$ , indicating wide IR transmission ranges (2.5–20 μm) (Fig. 4a and b). Several Raman peaks located at 300–500  $\text{cm}^{-1}$  are attributed to the Al-S bond interaction, such as (334, 374, 423, 500  $\text{cm}^{-1}$ ) for  $\text{LaCaAl}_3\text{S}_7$  and (334, 422, 498  $\text{cm}^{-1}$ ) for  $\text{LaSrAl}_3\text{S}_7$ , which are similar to those of other known thioaluminates, such as  $\text{K}(\text{AlS}_2)(\text{GeS}_2)$ <sup>62</sup> (375  $\text{cm}^{-1}$ ) and  $\text{Ba}_2\text{AlSbS}_5$ .<sup>63</sup> Other peaks located at 200–300  $\text{cm}^{-1}$  belong to the La-S bond vibration, which are similar to those of the previously reported  $\text{La}_2\text{S}_3$ .

Through the typical Kurtz-Perry method, we have investigated the powder SHG responses of  $\text{LaAeAl}_3\text{S}_7$  with different

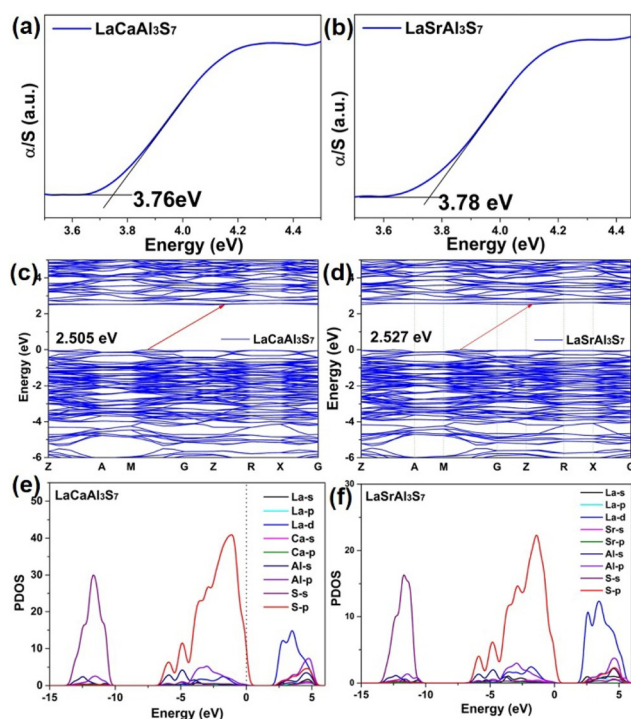


Fig. 3 Experimental optical bandgaps of  $\text{LaCaAl}_3\text{S}_7$  (a) and  $\text{LaSrAl}_3\text{S}_7$  (b); (c–f) band structures and PDOS of the title compounds.

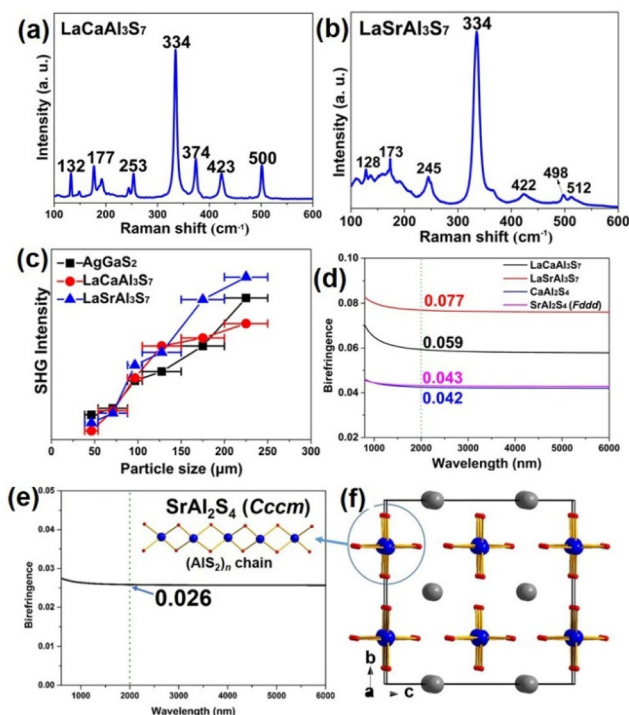


Fig. 4 Raman spectra of  $\text{LaCaAl}_3\text{S}_7$  (a) and  $\text{LaSrAl}_3\text{S}_7$  (b); (c) powder SHG response versus particle size for  $\text{LaAeAl}_3\text{S}_7$  with  $\text{AgGaS}_2$  as reference; (d) calculated birefringence for  $\text{LaAeAl}_3\text{S}_7$  and  $\text{AeAl}_2\text{S}_4$ ; (e) calculated birefringence for  $\text{Cccm-SrAl}_2\text{S}_4$ ; and (f) the 1D  $(\text{AlS}_2)_n$  chain in  $\text{Cccm-SrAl}_2\text{S}_4$ .

particle sizes under 2.09  $\mu\text{m}$  pulse laser and the as-synthesized  $\text{AgGaS}_2$  crystal as reference was selected. The measured results show that SHG intensity displays a similar growing trend with the increasing particle size. At the maximum particle size (200–250  $\mu\text{m}$ ), the title  $\text{LaAeAl}_3\text{S}_7$  possess large SHG responses about 0.8 times that of  $\text{AgGaS}_2$  for  $\text{LaCaAl}_3\text{S}_7$  and  $1.1 \times \text{AgGaS}_2$  for  $\text{LaSrAl}_3\text{S}_7$ , respectively (Fig. 4c), which are comparable to those of wide-bandgap NLO chalcogenides such as  $\text{LiZnPS}_4$ <sup>56</sup> ( $0.8 \times \text{AgGaS}_2$ ),  $\text{KYGes}_4$ <sup>39</sup> ( $1.0 \times \text{AgGaS}_2$ ),  $\text{Li}_{0.6}\text{Ag}_{0.4}\text{GaS}_2$ <sup>61</sup> ( $1.1 \times \text{AgGaS}_2$ ),  $\text{Na}_2\text{ZnGe}_2\text{S}_6$ <sup>64</sup> ( $0.9 \times \text{AgGaS}_2$ ) and  $[\text{Ba}_4\text{Cl}_2][\text{ZnGa}_4\text{S}_{10}]$ <sup>65</sup> ( $1.1 \times \text{AgGaS}_2$ ). In view of the fact that the NLO coefficient ( $d_{36}$ ) of  $\text{AgGaS}_2$  is  $13.0 \text{ pm V}^{-1}$ ,<sup>66</sup> we have also calculated the theoretical NLO coefficients ( $d_{ij}$ ) and their maximal  $d_{ij}$  are 6.83 for  $\text{LaCaAl}_3\text{S}_7$  and  $7.02 \text{ pm V}^{-1}$  for  $\text{LaSrAl}_3\text{S}_7$ , respectively, which are basically consistent with the experimental results. The origin of the NLO effect was analyzed by the SHG-density calculation and the results show that their NLO origin was derived from the synergistic effect between  $\text{AlS}_4$  and  $(\text{La}/\text{Ae})\text{S}_8$  anionic groups (Fig. 5). Note that the SHG responses ( $0.8\text{--}1.1 \times \text{AgGaS}_2$ ) of  $\text{LaAeAl}_3\text{S}_7$  are larger than that ( $0.5 \times \text{AgGaS}_2$ ) of  $\text{BaAl}_4\text{S}_7$ , which also further verifies that incorporation of lanthanide (Ln) atoms into crystal structures provides a great strategy to enhance the SHG response. Moreover, we have also calculated the birefringence *versus* wavelength curves for title the  $\text{LaAeAl}_3\text{S}_7$  and they exhibit a large optical anisotropy ( $\Delta n = 0.059$  for Ca and  $0.077$  for Sr@2  $\mu\text{m}$ ), such a large  $\Delta n$  also further verifies the rationality of experimental phase-matching (PM) behavior. Herein, we have also calculated the  $\Delta n$  of  $\text{CaAl}_2\text{S}_4$  (*Fddd*) and  $\text{SrAl}_2\text{S}_4$  (*Fddd* and *Cccm*) and the results show that *Fddd*- $\text{AeAl}_2\text{S}_4$  exhibit a relatively larger  $\Delta n$  (0.042 and 0.043) than that of *Cccm*- $\text{SrAl}_2\text{S}_4$  (0.026) (Fig. 4d). In general, the whole birefringence has a close relationship with the microscopic anisotropic polarizability of functional groups. In the title  $\text{LaAeAl}_3\text{S}_7$ , coplanar  $\text{AlS}_4$  units connect with each other to compose the Cairo pentagonal layers and such layered structures are beneficial to the optical anisotropy. We

have also calculated the contribution of anionic groups ( $\text{AlS}_4$  and  $(\text{La}/\text{Ae})\text{S}_8$ ) on the birefringences of title  $\text{LaAeAl}_3\text{S}_7$  by the real-space atom-cutting method and the calculated results show that the  $\text{AlS}_4$  unit provides the main contribution ( $\sim 76\%$ ) on the birefringence with a minor contribution ( $\sim 24\%$ ) of the  $(\text{La}/\text{Ca})\text{S}_8$  unit in  $\text{LaCaAl}_3\text{S}_7$ , which is similar to those in  $\text{LaSrAl}_3\text{S}_7$  ( $\text{AlS}_4$ : 80%;  $(\text{La}/\text{Sr})\text{S}_8$ : 20%). Besides, anisotropic distortions ( $\Delta d$ ) of  $(\text{La}/\text{Ae})\text{S}_8$  units in title  $\text{LaAeAl}_3\text{S}_7$  are much larger than those of  $\text{AeAl}_2\text{S}_4$ , which also contributes to the improvement of birefringence. Thus, the microscopic addition of  $\text{AlS}_4$  and  $(\text{La}/\text{Ae})\text{S}_8$  groups makes the  $\text{LaAeAl}_3\text{S}_7$  exhibit a relatively larger optical anisotropy than those of *Fddd*- $\text{AeAl}_2\text{S}_4$  (2D layer), *Cccm*- $\text{SrAl}_2\text{S}_4$  ( $(\text{AlS}_2)_n$  chain) (Fig. 4e and f) and  $\text{BaAl}_4\text{S}_7$  ( $\Delta n = 0.0328$ , 3D network) since the contribution of alkaline-earth cations on birefringence is negligible. Therefore, combination of Cairo pentagonal layers and lanthanides into crystal structures is conducive to improving optical anisotropy, which provides a useful structure-directing design for the discovery of new potential PM NLO crystals. To sum up, considering the overall performances of title  $\text{LaAeAl}_3\text{S}_7$ , they exhibit wide bandgaps ( $E_g$ : 3.76–3.78 eV), large SHG responses ( $d_{ij}$ :  $0.8\text{--}1.1 \times \text{AgGaS}_2$ ), high LDTs ( $9.0 \times \text{AgGaS}_2$ ) and good chemical stability, indicating that title  $\text{LaAeAl}_3\text{S}_7$  could be viewed as the first cases satisfying the excellent property balance ( $E_g > 3.5 \text{ eV}$  and  $d_{ij} > 0.5 \times \text{AgGaS}_2$ ) in rare-earth NLO chalcogenides.

## Conclusions

In summary, two new  $\text{LaAeAl}_3\text{S}_7$  thioaluminates were firstly synthesized and their measured performances verify them to be potential IR NLO candidates. Synergistic contributions between  $(\text{La}/\text{Ae})\text{S}_8$  and  $\text{AlS}_4$  units afford strong NLO responses in  $\text{LaAeAl}_3\text{S}_7$ . The novel Cairo pentagonal layered structures in  $\text{LaAeAl}_3\text{S}_7$  have the benefit of improving the optical anisotropy, which provides a structure-directing strategy for the discovery of PM crystals. This study indicates that Ln-based thioaluminates could be expected to be feasible research systems for the breakthrough in the incompatibility between a strong SHG response and a wide bandgap to achieve the imperative property balance.

## Author contributions

The manuscript was written through contributions of all authors. All authors have given approval to the final version of the manuscript.

## Conflicts of interest

There are no conflicts to declare.

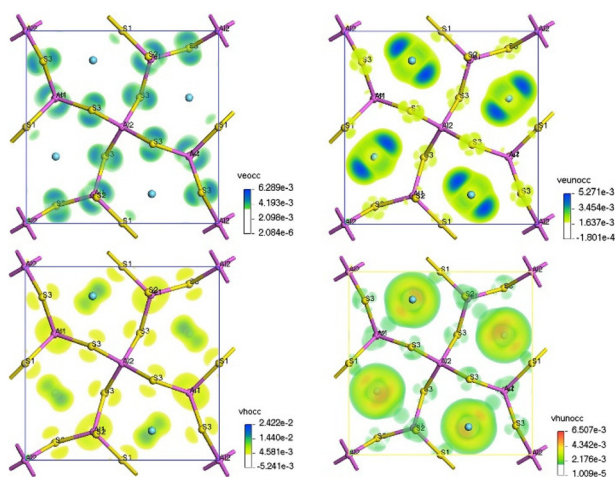


Fig. 5 Calculated SHG-density diagrams in the occupied and unoccupied states of  $\text{LaAeAl}_3\text{S}_7$ .

## Acknowledgements

This work was supported by the National Natural Science Foundation of China (Grant No. 51872324) and the Natural Science Foundation of Hebei Province (Grant No. E2020201005).

## References

- 1 F. You, F. Liang, Q. Huang, Z. Hu, Y. Wu and Z. Lin,  $\text{Pb}_2\text{GaF}_2(\text{SeO}_3)_2\text{Cl}$ : Band Engineering Strategy by Aliovalent Substitution for Enlarging Bandgap while Keeping Strong Second Harmonic Generation Response, *J. Am. Chem. Soc.*, 2018, **141**, 748–752.
- 2 S. P. Guo, X. Cheng, Z. D. Sun, Y. Chi, B. W. Liu, X. M. Jiang, S. F. Li, H. G. Xue, S. Deng, V. Duppel and G. C. Guo, Large Second Harmonic Generation (SHG) Effect and High Laser-Induced Damage Threshold (LIDT) Observed Coexisting in Gallium Selenide, *Angew. Chem., Int. Ed.*, 2019, **58**, 8087–8091.
- 3 H. Lin, B.-X. Li, H. Chen, P.-F. Liu, L.-M. Wu, X.-T. Wu and Q.-L. Zhu,  $\text{Sr}_5\text{ZnGa}_6\text{S}_{15}$ : a new quaternary non-centrosymmetric semiconductor with a 3D framework structure displaying excellent nonlinear optical performance, *Inorg. Chem. Front.*, 2018, **5**, 1458–1462.
- 4 Y. Xiao, M.-M. Chen, Y.-Y. Shen, P.-F. Liu, H. Lin and Y. Liu,  $\text{A}_3\text{Mn}_2\text{Sb}_3\text{S}_8$  (A = K and Rb): a new type of multifunctional infrared nonlinear optical material based on unique three-dimensional open frameworks, *Inorg. Chem. Front.*, 2021, **8**, 2835–2843.
- 5 Y. J. Jia, Y. G. Chen, Y. Guo, X. F. Guan, C. Li, B. Li, M. M. Liu and X. M. Zhang,  $\text{LiM}^{\text{II}}(\text{IO}_3)_3$  ( $\text{M}^{\text{II}} = \text{Zn}$  and  $\text{Cd}$ ): Two Promising Nonlinear Optical Crystals Derived from a Tunable Structure Model of  $\alpha\text{-LiIO}_3$ , *Angew. Chem., Int. Ed.*, 2019, **58**, 17194–17198.
- 6 J. Huang, J. Cheng, B.-H. Lei, Z. Wei, S. Pan and Z. Yang, Synergism of multiple functional chromophores significantly enhancing the birefringence in layered non-centrosymmetric chalcogenides, *Inorg. Chem. Front.*, 2021, **8**, 1588–1598.
- 7 T. K. Bera, J. I. Jang, J. B. Ketterson and M. G. Kanatzidis, Strong second harmonic generation from the tantalum thioarsenates  $\text{A}_3\text{Ta}_2\text{AsS}_{11}$  (A = K and Rb), *J. Am. Chem. Soc.*, 2009, **131**, 75–77.
- 8 Y.-J. Lin, B.-W. Liu, R. Ye, X.-M. Jiang, L.-Q. Yang, H.-Y. Zeng and G.-C. Guo,  $\text{SrCdSnQ}_4$  (Q = S and Se): infrared nonlinear optical chalcogenides with mixed NLO-active and synergetic distorted motifs, *J. Mater. Chem. C*, 2019, **7**, 4459–4465.
- 9 V. Nguyen, B. Ji, K. Wu, B. Zhang and J. Wang, Unprecedented mid-infrared nonlinear optical materials achieved by crystal structure engineering, a case study of  $(\text{KX})\text{P}_2\text{S}_6$  (X = Sb, Bi, Ba), *Chem. Sci.*, 2022, **13**, 2640–2648.
- 10 X. Dong, L. Huang, H. Zeng, Z. Lin, K. M. Ok and G. Zou, High-Performance Sulfate Optical Materials Exhibiting Giant Second Harmonic Generation and Large Birefringence, *Angew. Chem., Int. Ed.*, 2022, **61**, e202116790.
- 11 X. Chen, Q. Jing and K. M. Ok,  $\text{Pb}_{18}\text{O}_8\text{Cl}_{15}\text{I}_5$ : A polar Lead mixed oxyhalide with unprecedented architecture and excellent infrared nonlinear optical properties, *Angew. Chem., Int. Ed.*, 2020, **59**, 20323–20327.
- 12 Y. Zhou, Y. Li, Q. Ding, Y. Liu, Y. Chen, X. Liu, X. Huang, L. Li, S. Zhao and J. Luo, Noncentrosymmetric  $\text{K}_2\text{Mn}_3(\text{SO}_4)_3\text{F}_2 \cdot 4\text{H}_2\text{O}$  and  $\text{Rb}_2\text{Mn}_3(\text{SO}_4)_3\text{F}_2 \cdot 2\text{H}_2\text{O}$  with pseudo-KTP structures, *Chin. Chem. Lett.*, 2021, **32**, 263–265.
- 13 Y. Liu, Y. Liu, Z. Lin, Y. Li, Q. Ding, X. Chen, L. Li, S. Zhao, M. Hong and J. Luo, Nonpolar  $\text{Na}_{10}\text{Cd}(\text{NO}_3)_4(\text{SO}_3\text{S})_4$  Exhibits a Large Second-Harmonic Generation, *CCS Chem.*, 2022, **4**, 526–531.
- 14 Y. Li, W. Huang, Y. Zhou, X. Song, J. Zheng, H. Wang, Y. Song, M. Li, J. Luo and S. Zhao, A High-Performance Nonlinear Optical Crystal with a Building Block Containing Expanded  $\pi$ -Delocalization, *Angew. Chem., Int. Ed.*, 2023, **62**, e202215145.
- 15 M. Li, X. Zhang, Z. Xiong, Y. Li, Y. Zhou, X. Chen, Y. Song, M. Hong, J. Luo and S. Zhao, A Hybrid Antiperovskite with Strong Linear and Second-Order Nonlinear Optical Responses, *Angew. Chem., Int. Ed.*, 2022, **61**, e202211151.
- 16 Y. Chu, P. Wang, H. Zeng, S. Cheng, X. Su, Z. Yang, J. Li and S. Pan,  $\text{Hg}_3\text{P}_2\text{S}_8$ : a new promising infrared nonlinear optical material with a large second-harmonic generation and a high laser-induced damage threshold, *Chem. Mater.*, 2021, **33**, 6514–6521.
- 17 I. Chung and M. G. Kanatzidis, Metal chalcogenides: a rich source of nonlinear optical materials, *Chem. Mater.*, 2014, **26**, 849–869.
- 18 H. Zhang, M. Zhang, S. Pan, X. Dong, Z. Yang, X. Hou, Z. Wang, K. B. Chang and K. R. Poeppelmeier,  $\text{Pb}_{17}\text{O}_8\text{Cl}_{18}$ : A promising IR nonlinear optical material with large laser damage threshold synthesized in an open system, *J. Am. Chem. Soc.*, 2015, **137**, 8360–8363.
- 19 A. G. Jackson, M. C. Ohmer and S. R. LeClair, Relationship of the second order nonlinear optical coefficient to energy gap in inorganic non-centrosymmetric crystals, *Infrared Phys. Technol.*, 1997, **38**, 233–244.
- 20 G. Boyd, H. Kasper and J. McFee, Linear and nonlinear optical properties of  $\text{AgGaS}_2$ ,  $\text{CuGaS}_2$ , and  $\text{CuInS}_2$ , and theory of the wedge technique for the measurement of nonlinear coefficients, *IEEE J. Quantum Electron.*, 1971, **7**, 563–573.
- 21 B. Tell and H. Kasper, Optical and electrical properties of  $\text{AgGaS}_2$  and  $\text{AgGaSe}_2$ , *Phys. Rev. B: Solid State*, 1971, **4**, 4455.
- 22 G. Boyd, E. Buehler and F. Storz, Linear and nonlinear optical properties of  $\text{ZnGeP}_2$  and  $\text{CdSe}$ , *Appl. Phys. Lett.*, 1971, **18**, 301–304.
- 23 K. Wu and S. Pan, A review on structure-performance relationship toward the optimal design of infrared nonlinear optical materials with balanced performances, *Coord. Chem. Rev.*, 2018, **377**, 191–208.

- 24 S. Guo, Y. Chi and G. Guo, Recent achievements on middle and far-infrared second-order nonlinear optical materials, *Coord. Chem. Rev.*, 2017, **335**, 44–57.
- 25 Y. Li, W. Wang, H. Wang, H. Lin and L. Wu, Mixed-anion inorganic compounds: a favorable candidate for infrared nonlinear optical materials, *Cryst. Growth Des.*, 2019, **19**, 4172–4192.
- 26 H. Yang, M. Ran, S. Zhou, X. Wu, H. Lin and Q. Zhu, Rational design via dual-site aliovalent substitution leads to an outstanding IR nonlinear optical material with well-balanced comprehensive properties, *Chem. Sci.*, 2022, **13**, 10725–10733.
- 27 H. Lin, W. Wei, H. Chen, X. Wu and Q. Zhu, Rational design of infrared nonlinear optical chalcogenides by chemical substitution, *Coord. Chem. Rev.*, 2020, **406**, 213150.
- 28 L. Gao, J. Huang, S. Guo, Z. Yang and S. Pan, Structure-property survey and computer-assisted screening of mid-infrared nonlinear optical chalcogenides, *Coord. Chem. Rev.*, 2020, **421**, 213379.
- 29 W. Wang, D. Mei, F. Liang, J. Zhao, Y. Wu and Z. Lin, Inherent laws between tetrahedral arrangement pattern and optical performance in tetrahedron-based mid-infrared nonlinear optical materials, *Coord. Chem. Rev.*, 2020, **421**, 213444.
- 30 S. P. Guo, G. C. Guo and J. Huang, Syntheses, structures and properties of five chiral quaternary sulfides,  $Al_xLn_3(Si_yAl_{1-y})S_7$  ( $Ln = Y, Gd, Dy$ ) and  $In_{0.33}Sm_3SiS_7$ , *Sci. China, Ser. B: Chem.*, 2009, **52**, 1609–1615.
- 31 S.-P. Guo, G.-C. Guo, M.-S. Wang, J.-P. Zou, G. Xu, G.-J. Wang, X.-F. Long and J.-S. Huang, A Series of New Infrared NLO Semiconductors,  $ZnY_6Si_2S_{14}$ ,  $Al_xDy_3(Si_yAl_{1-y})S_7$ , and  $Al_{0.33}Sm_3SiS_7$ , *Inorg. Chem.*, 2009, **48**, 7059–7065.
- 32 D. Mei, J. Jiang, F. Liang, S. Zhang, Y. Wu, C. Sun, D. Xue and Z. Lin, Design and synthesis of a nonlinear optical material  $BaAl_4S_7$  with a wide band gap inspired from  $SrB_4O_7$ , *J. Mater. Chem. C*, 2018, **6**, 2684–2689.
- 33 G. Li, Z. Yang and S. Pan,  $LiAlS_2$ : A promising infrared frequency-conversion material with ultrawide band gap and high laser-induced damage threshold, *Sci. China Mater.*, 2022, **1**–8.
- 34 L. Zhou, L. Chen, J. Li and L. Wu, First-principles studies on linear and nonlinear optical effects in  $Ln_4GaSbS_9$  ( $Ln = Ce-Nd, Sm, Gd-Tm, Lu$ ), *J. Solid State Chem.*, 2012, **195**, 166–171.
- 35 H. Lin, Y. Li, M. Li, Z. Ma, L. Wu, X. Wu and Q. Zhu, Centric-to-acentric structure transformation induced by a stereochemically active lone pair: a new insight for design of IR nonlinear optical materials, *J. Mater. Chem. C*, 2019, **7**, 4638–4643.
- 36 H. Zhao, Synthesis, crystal structure, and NLO property of the chiral sulfide  $Sm_4InSbS_9$ , *Z. Anorg. Allg. Chem.*, 2016, **642**, 56–59.
- 37 M. J. Zhang, B. X. Li, B. W. Liu, Y. H. Fan, X. G. Li, H. Y. Zeng and G. C. Guo,  $Ln_3GaS_6$  ( $Ln = Dy, Y$ ): new infrared nonlinear optical materials with high laser induced damage thresholds, *Dalton Trans.*, 2013, **42**, 14223–14229.
- 38 Y. Yang, Y. Chu, B. Zhang, K. Wu and S. Pan, Unique Unilateral-Chelated Mode-Induced d-p- $\pi$  Interaction Enhances Second-Harmonic Generation Response in New  $Ln_3LiMS_7$  Family, *Chem. Mater.*, 2021, **33**, 4225–4230.
- 39 D. Mei, W. Cao, N. Wang, X. Jiang, J. Zhao, W. Wang, J. Dang, S. Zhang, Y. Wu, P. Rao and Z. Lin, Breaking through the “3.0 eV wall” of energy band gap in mid-infrared nonlinear optical rare earth chalcogenides by charge-transfer engineering, *Mater. Horiz.*, 2021, **8**, 2330–2334.
- 40 H. J. Zhao, Y. F. Zhang and L. Chen, Strong Kleinman-forbidden second harmonic generation in chiral sulfide:  $La_4InSbS_9$ , *J. Am. Chem. Soc.*, 2012, **134**, 1993–1995.
- 41 W. Xing, C. Tang, N. Wang, C. Li, Z. Li, J. Wu, Z. Lin, J. Yao, W. Yin and B. Kang,  $EuHgGeSe_4$  and  $EuHgSnS_4$ : Two Quaternary Eu-Based Infrared Nonlinear Optical Materials with Strong Second-Harmonic-Generation Responses, *Inorg. Chem.*, 2020, **59**, 18452–18460.
- 42 H. J. Zhao and L. J. Zhou, A Series of Noncentrosymmetric Antimony Sulfides  $Ln_8Sb_2S_{15}$  ( $Ln = La, Pr, Nd$ ) – Syntheses, Crystal and Electronic Structures, and NLO Properties, *Eur. J. Inorg. Chem.*, 2015, **2015**, 964–968.
- 43 Y.-F. Shi, Y.-K. Chen, M.-C. Chen, L.-M. Wu, H. Lin, L.-J. Zhou and L. Chen, Strongest Second Harmonic Generation in the Polar  $R_3MTQ_7$  Family: Atomic Distribution Induced Nonlinear Optical Cooperation, *Chem. Mater.*, 2015, **27**, 1876–1884.
- 44 Q. G. Yue, S. H. Zhou, B. Li, X. T. Wu, H. Lin and Q. L. Zhu, Quaternary Noncentrosymmetric Rare-Earth Sulfides  $Ba_4RE_2Cd_3S_{10}$  ( $RE = Sm, Gd, or Tb$ ): A Joint Experimental and Theoretical Investigation, *Inorg. Chem.*, 2022, **61**, 1797–1804.
- 45 J. Xu, K. Wu, Y. Xiao, B. Zhang, H. Yu and H. Zhang, Mixed-Anion-Oriented Design of  $LnMGa_3S_6O$  ( $Ln = La, Pr, and Nd$ ;  $M = Ca$  and  $Sr$ ) Nonlinear Optical Oxsulfides with Targeted Property Balance, *ACS Appl. Mater. Interfaces*, 2022, **14**, 37967–37974.
- 46 W. Xing, N. Wang, Y. Guo, Z. Li, J. Tang, K. Kang, W. Yin, Z. Lin, J. Yao and B. Kang, Two rare-earth-based quaternary chalcogenides  $EuCdGeQ_4$  ( $Q = S, Se$ ) with strong second-harmonic generation, *Dalton Trans.*, 2019, **48**, 17620–17625.
- 47 M. C. Chen, L. H. Li, Y. B. Chen and L. Chen, In-phase alignments of asymmetric building units in  $Ln_4GaSbS_9$  ( $Ln = Pr, Nd, Sm, Gd-Ho$ ) and their strong nonlinear optical responses in middle IR, *J. Am. Chem. Soc.*, 2011, **133**, 4617–4624.
- 48 M. Usman, M. D. Smith, G. Morrison, V. V. Klepov, W. Zhang, P. S. Halasyamani and H. C. Zur Loye, Molten Alkali Halide Flux Growth of an Extensive Family of Noncentrosymmetric Rare Earth Sulfides: Structure and Magnetic and Optical (SHG) Properties, *Inorg. Chem.*, 2019, **58**, 8541–8550.

- 49 V. Winkler, M. Schlosser and A. Pfitzner, Synthesis and Crystal Structures of  $\text{Rb}_4\text{Al}_2\text{S}_5$  and  $\text{Cs}_4\text{In}_2\text{S}_5$ , *Z. Anorg. Allg. Chem.*, 2015, **641**, 549–556.
- 50 H. Kalpen, W. Honle, M. Somer, U. Schwarz, K. Peters, H. Von Schnering and R. Blachnik, Bismuth(II) chalcogenometallates (III)  $\text{Bi}_2\text{M}_4\text{X}_8$ , compounds with Bi-2 (4+) dumbbells (M = Al, Ga and X = S, Se), *Z. Anorg. Allg. Chem.*, 1998, **624**, 1137–1147.
- 51 R. Eholie, O. Gorochoy, M. Guittard, A. Mazurier and J. Flahaut, Les composés de type  $\text{PbGa}_2\text{Se}_4$ ,  $\text{EuM}_2\text{X}_4$ ,  $\text{SrM}_2\text{X}_4$  and  $\text{PbM}_2\text{X}_4$ , *Bull. Soc. Chim. Fr.*, 1971, **3**, 747–750.
- 52 M. Patrie and M. Guittard, Compounds of type  $\text{Ce}_6\text{Al}_{10/3}\text{S}_{14}$ , *C. R. Hebd. Seances Acad. Sci.*, 1969, **268**, 1136–1138.
- 53 L. Duan, X. Wang, J. Zhao, J. Zhang, S. Du, Y. Feng, Z. Zhao, S. Wang and C. Jin, High-Pressure Synthesis and Physical Properties of a Spinel Compound  $\text{FeAl}_2\text{S}_4$ , *Inorg. Chem.*, 2022, **61**, 13184–13190.
- 54 D. Muller, F. Poltman and H. Hahn, Zur-Struktur ternäre Chalkogenide des Thalliums mit Aluminium, Gallium und Indium, *Z. Naturforsch.*, 1974, **29**, 117–118.
- 55 B. Eisenmann, M. Jakowski, W. Klee and H. Schaefer, Structures of calcium aluminum sulfide ( $\text{CaAl}_2\text{S}_4$ ), calcium gallium sulfide ( $\text{CaGa}_2\text{S}_4$ ), strontium aluminum sulfide ( $\text{SrAl}_2\text{S}_4$ ), strontium gallium sulfide ( $\text{SrGa}_2\text{S}_4$ ) and barium indium sulfide ( $\text{BaIn}_2\text{S}_4$ ), *Chem. Inf.*, 1983, **14**, 255–263.
- 56 M. Zhou, L. Kang, J. Yao, Z. Lin, Y. Wu and C. Chen, Midinfrared nonlinear optical thiophosphates from  $\text{LiZnPS}_4$  to  $\text{AgZnPS}_4$ : a combined experimental and theoretical study, *Inorg. Chem.*, 2016, **55**, 3724–3726.
- 57 B.-W. Liu, H.-Y. Zeng, X.-M. Jiang, G.-E. Wang, S.-F. Li, L. Xu and G.-C. Guo,  $[\text{A}_3\text{X}][\text{Ga}_3\text{PS}_8]$  (A = K, Rb; X = Cl, Br): promising IR non-linear optical materials exhibiting concurrently strong second-harmonic generation and high laser induced damage thresholds, *Chem. Sci.*, 2016, **7**, 6273–6277.
- 58 W. Yin, K. Feng, R. He, D. Mei, Z. Lin, J. Yao and Y. Wu,  $\text{BaGa}_2\text{MQ}_6$  (M = Si, Ge; Q = S, Se): a new series of promising IR nonlinear optical materials, *Dalton Trans.*, 2012, **41**, 5653–5661.
- 59 G. Li, Y. Chu and Z. Zhou, From  $\text{AgGaS}_2$  to  $\text{Li}_2\text{ZnSiS}_4$ : realizing impressive high laser damage threshold together with large second-harmonic generation response, *Chem. Mater.*, 2018, **30**, 602–606.
- 60 Y. Kim, I. S. Seo, S. W. Martin, J. Baek, P. Shiv Halasyamani, N. Arumugam and H. Steinfink, Characterization of new infrared nonlinear optical material with high laser damage threshold,  $\text{Li}_2\text{Ga}_2\text{GeS}_6$ , *Chem. Mater.*, 2008, **20**, 6048–6052.
- 61 H. Zhou, L. Xiong, L. Chen and L. Wu, Size match reducing dislocations within lattice leads to ultrawide band gap, large second order susceptibility and high nonlinear optical performance of  $\text{AgGaS}_2$ , *Angew. Chem., Int. Ed.*, 2019, **58**, 9979–9983.
- 62 M. Al-Bloushi, B. Davaasuren, A.-H. Emwas and A. Rothenberger, Synthesis and Characterization of the Quaternary Thio-aluminogermanates  $\text{A}(\text{AlS}_2)(\text{GeS}_2)$  (A = Na, K), *Z. Anorg. Allg. Chem.*, 2015, **641**, 1352–1356.
- 63 X. Wu, X. Gu, H. Pan, Y. Hu and K. Wu, Synthesis, Crystal Structures, Optical Properties and Theoretical Calculations of Two Metal Chalcogenides  $\text{Ba}_2\text{AlSbS}_5$  and  $\text{Ba}_2\text{GaBiSe}_5$ , *Crystals*, 2018, **8**, 165.
- 64 G. Li, K. Wu, Q. Liu, Z. Yang and S. Pan,  $\text{Na}_2\text{ZnGe}_2\text{S}_6$ : a new infrared nonlinear optical material with good balance between large second-harmonic generation response and high laser damage threshold, *J. Am. Chem. Soc.*, 2016, **138**, 7422–7428.
- 65 H. Chen, Y.-Y. Li, B. Li, P.-F. Liu, H. Lin, Q.-L. Zhu and X.-T. Wu, Salt-inclusion chalcogenide  $[\text{Ba}_4\text{Cl}_2][\text{ZnGa}_4\text{S}_{10}]$ : rational design of an IR nonlinear optical material with superior comprehensive performance derived from  $\text{AgGaS}_2$ , *Chem. Mater.*, 2020, **32**, 8012–8019.
- 66 V. V. Badikov, O. N. Pivovarov, Yu. V. Skokov, O. V. Skrebneva and N. K. Trotsenko, Some optical properties of silver thiogallate single crystals, *Sov. J. Quantum. Electron.*, 1975, **5**, 618–621.